

The large-scale environment of FR 0 radio galaxies.

A. Capetti¹, F. Massaro^{2,1,3,4}, and R. D. Baldi^{2,5}

¹ INAF-Osservatorio Astrofisico di Torino, via Osservatorio 20, 10025 Pino Torinese, Italy,

² Dipartimento di Fisica, Università degli Studi di Torino, via Pietro Giuria 1, 10125 Torino, Italy,

³ Istituto Nazionale di Fisica Nucleare, Sezione di Torino, I- 10125 Torino, Italy,

⁴ Consorzio Interuniversitario per la Fisica Spaziale, via Pietro Giuria 1, I-10125 Torino, Italy,

⁵ Department of Physics and Astronomy, University of Southampton, Highfield, SO17 1BJ, UK

ABSTRACT

We explore the properties of the large-scale environment of FR 0 radio galaxies belonging to the FROCAT sample which includes 104 compact radio sources associated with nearby ($z < 0.05$) early-type galaxies. By using various estimators we find that FR 0s live in regions of higher than the average galaxies density and a factor two lower density, on average, with respect to FR I radio galaxies. This latter difference is driven by the large fraction (63%) of FR 0s located in groups formed by less than 15 galaxies, an environment which FR Is rarely (17%) inhabit. Beside the lack of substantial extended radio emission defining the FR 0s class, this is the first significant difference between the properties of these two populations of low power radio galaxies. We interpret the differences in environment between FR 0s and FR Is as the due to an evolutionary link between local galaxies density, BH spin, jet power, and extended radio emission.

Key words. galaxies: active – galaxies: jets

1. Introduction

The connection between the large scale environment and the properties of extra-galactic radio sources has been explored since the '70s (e.g., Longair & Seldner 1979). Longair & Seldner found that weak radio galaxies (RGs) show no tendency to belong to groups or clusters of galaxies, an environment which is instead typical of extended powerful radio sources. Prestage & Peacock (1988) claimed that Fanaroff-Riley class II sources (Fanaroff & Riley, 1974), FR IIs, as well as compact radio sources, lie on average in poorer clusters than those of class I (FR Is). Hill & Lilly (1991) found a strong evolution of the RGs environment, because already at $z = 0.5$ most powerful sources are located in rich clusters, unlike what is seen at lower redshifts.

Several radio surveys covering large areas and reaching the mJy flux level became available in the last two decades, e.g., FIRST (Becker et al., 1995; Helfand et al., 2015) and NVSS (Condon et al., 1998). The studies of the RGs environment based on these surveys broadly confirmed the earlier results. Best (2004) found that radio-AGN are preferentially located in galaxy groups and poor-to-moderate richness galaxy clusters. Gendre et al. (2013) provided further support to the higher local galaxies density around FR Is with respect to FR IIs; they also noted the possible presence of a link between the various optical classes of RGs (Laing et al., 1994): high-excitation galaxies (HEGs) are found almost exclusively in low-density environments while low-excitation galaxies (LEGs) occupy a wider range of densities. By using observations from the International Low Frequency Array (LOFAR; van Haarlem et al. 2013) Croston et al. (2019) found a connection between size and luminosity at 150 MHz of the brightest radio AGN with the cluster richness. In contrast, Massaro et al. (2019a), hereafter M19, concluded that regardless of their radio morphological classification (FR I or FR II) and/or their optical classification (LEGs of

HEGs) RGs in the local universe live in galaxy-rich large-scale environments that have similar characteristics and richness. This different result is probably driven by the different selection criteria of the samples.

These studies focused almost exclusively on the bright extended RGs. However, the identification of the optical counterparts of radio sources (Best et al., 2005; Best & Heckman, 2012) in FIRST and NVSS showed that the majority of them are associated with low redshift galaxies and are unresolved (Baldi & Capetti, 2009). This is a radical change in our view of the radio sky, because earlier surveys (performed at lower frequency and higher flux threshold) were dominated by sources extending over a typical scale of hundreds of kpc (e.g., Hardcastle et al. 1998). The general lack of substantial extended radio emission suggested to define these “compact” sources as “FR 0s” (Ghisellini, 2011; Sadler et al., 2014), as a convenient way to include them into the canonical Fanaroff & Riley (1974) classification scheme of radio galaxies (RGs).

The information on FR 0s is quite limited, even at the radio frequencies used to classify them: the available radio data are of poor resolution and with multi frequency data available only for the FR 0s of higher flux density. As a consequence, it is still unclear which is the nature of these compact sources and how they are related to the other classes of RGs. In order to perform a systematic studies of FR 0s, Baldi et al. (2018), hereafter BCM18, selected a sample of 104 compact radio sources, named FROCAT, while Capetti et al. (2017) built a comparison sample of extended, edge-darkened FR I RGs (see Sect. 2 for further details on the samples selection). The number density of FROCAT sources is five times higher than that of FR Is, confirming quantitatively that they represent the dominant population of radio sources in the local Universe (BCM18). Baldi et al. found that the FROCAT hosts are mostly luminous red early-type galaxies with large black hole masses ($10^8 \lesssim M_{\text{BH}} \lesssim 10^9 M_{\odot}$). These properties are similar to those seen for the hosts of FR Is, they

are just on average a factor 1.6 less massive but there is a large overlap between the two mass distributions.

Baldi et al. (2015, 2019) obtained high resolution multi-frequency radio images of a sub sample of FR 0s extracted from FR0CAT. Although they reach an angular resolution of $0''.3$ (corresponding to a few hundred pc), the majority of the FR 0s are still unresolved, while the remaining extend only a few kpc. Most of them have flat spectra and the ratio between the core and total emission in FR 0s is ~ 30 times higher than that in FR Is.

The comparison of optical line emission luminosity, a robust proxy of the radiative power of the AGN, indicates that FR 0s share the same range of FR Is, but they have a median radio luminosity a factor ~ 30 smaller than that of the FRICAT (BCM18). However, there is no sharp boundary between the properties of FR 0s and FR Is: low-luminosity RGs form a continuous distribution, from the FR 0s at the lowest ratios of radio/line luminosity, to the FRICAT sources at intermediate ratios, and finally to the extreme values reached by the most powerful FR Is part of the Third Cambridge catalog (Spinrad et al., 1985). If we instead consider only the emission from the radio core, the FR 0s lie in the same region populated by the FR Is, indicating a common nature of the nuclei of the two groups of sources. This similarity is also supported by available X-rays observations (Torresi et al., 2018).

It therefore appears that, while the host galaxies and the nuclear properties of FR 0s and FR Is are very similar, their appearance in the radio images is radically different. The origin of their different nature still remains to be understood. For example, a scenario in which FR 0s are young RGs that will all eventually evolve into extended radio sources cannot be reconciled with the large space density of FR 0s. FR 0s might instead be recurrent sources, characterized by short phases of activity (BCM18). Finally, the jet properties of FR 0s might be intrinsically different from those of the FR Is, e.g., the former class having lower bulk Lorentz factors (Baldi et al., 2019). The VLBI observations obtained by Cheng & An (2018) indicate a diversity of relativistic beaming indicators among the sources of the sub-sample of 14 bright (with flux densities > 50 mJy) FR 0s they analyzed.

In this work we extend our comparison of FR 0s and FR Is by studying their large-scale environment, probing distances up to 2 Mpc, testing whether their different radio morphologies are related to, e.g., the local densities of galaxies. The paper is organized as follows: in Sect. 2 we describe the samples considered and whose environment is studied in Sect. 3. The results are discussed in Sect. 4, while our conclusions are given in Sect. 5.

Throughout the paper we assume the same cosmology as in M19, i.e., $H_0 = 69.6 \text{ km s}^{-1} \text{ Mpc}^{-1}$, $\Omega_M = 0.286$, and $\Omega_\Lambda = 0.714$ (Bennett et al., 2014). Thus, $1''$ corresponds to 0.984 kpc at $z = 0.05$.

2. The samples

The three samples of RGs we selected for the comparison of their large-scale (up to 2 Mpc) environmental properties are those formed by the compact FR0CAT sources with $z < 0.05$, and the two catalogs of edge-darkened sources, FRICAT, and sFRICAT, limiting to those with the same redshift limit of the FR 0s.

We recently created a catalog of 219 FR Is (FRICAT, Capetti et al. 2017) starting from the list of radio AGN produced by Best & Heckman (2012). We visually inspected the FIRST image for each individual source with $z < 0.15$ selecting those having radio emission with an edge darkened morphology. We

initially considered only those extending to a radius r larger than 30 kpc, i.e., well resolved sources at the $5''$ resolution of the FIRST images within the redshift range of interest. Capetti et al. (2017) also considered a second sample of 14 smaller FR Is (hereafter sFRICAT), having $10 < r < 30 \text{ kpc}$, but limiting to the objects with $z < 0.05$ to preserve a sufficient spatial resolution. The final sample of low redshift FR Is is composed by 23 objects, the 9 FRICAT with $z < 0.05$ and the 14 sFRICAT. From the point of view of the optical spectroscopic classification, all FRICAT and sFRICAT sources are low excitation galaxies (LEGs).

FR0CAT is instead composed by 104 compact RGs (BCM18).¹ They have been selected from the Best & Heckman catalog, imposing a redshift limit of 0.05. We set a limit to the maximum deconvolved size of $4''$, corresponding to a size $r \lesssim 2.5 \text{ kpc}$. We also required an optical spectroscopic classification as LEGs.

In the Appendix we provide three tables where we list the main properties of the samples studied.

The redshift distributions of the samples considered are not statistically distinguishable, with an average value of 0.037 for the FR 0s and 0.036 for the FR Is (see Fig. 1, left panel, and Table 1). Conversely, as already noted by BCM18, the FR Is hosts are 0.66 magnitudes brighter than those of FR 0s (Fig. 1, right panel).

Following M19, in our analysis we also used a catalog of mock sources (labeled as MOCK hereinafter) to estimate the efficiency of our procedures. This has been created by shifting the positions of the FRICAT sources by a random radius between 2° and 3° while preserving their redshift distribution. The MOCK sample lists 4056 sources, 278 of which have $z < 0.05$. The MOCK sample provides us with a description of the environmental properties of random locations in the local Universe to be compared with those derived from the sources of our interest.

3. Environmental properties

3.1. Estimates of the local galaxies density

M19 studied the environment of the sub sample 195 FRICAT sources lying in the central part of the SDSS footprint (see, e.g., Ahn et al. 2012), the area covered by the catalog of groups and clusters of galaxies produced by Tempel et al. (2012), hereinafter T12, which was used as reference for their analysis.

M19 defined as “cosmological neighbors” all galaxies lying within a region of given projected radius (they mostly used a radius of 2 Mpc) and having a spectroscopic redshift z differing by less than 0.005 from the radio galaxy in the center of the field examined. This choice corresponds to the maximum velocity dispersion in groups and clusters of galaxies (see, e.g., Eke et al. 2004). At the average redshift of the samples of RGs, 0.037, the spectroscopic limit of the SDSS ($m_r=17.7$) corresponds to an absolute magnitude of $M_r=-18.4$. This luminosity is well below the peak in the luminosity function of elliptical galaxies (e.g., Tempel et al. 2011) and ~ 4 magnitudes below the median optical luminosity of both FR 0s and FR Is: at these low redshifts the SDSS provides us with detailed information on environment.

The number of cosmological neighbors within 2 Mpc, N_{cn}^{2000} , spans a large range, reaching values as high as 164, see Fig. 2. The median values of N_{cn}^{2000} is 13 for the FR 0s and 44 for the

¹ The initial FR0CAT sample was formed by 108 objects. The inspection of their NVSS images revealed the presence of low brightness diffuse emission, resolved out in the FIRST images, in four of them, that have then been removed from the catalog (see Baldi et al. 2019 for further details).

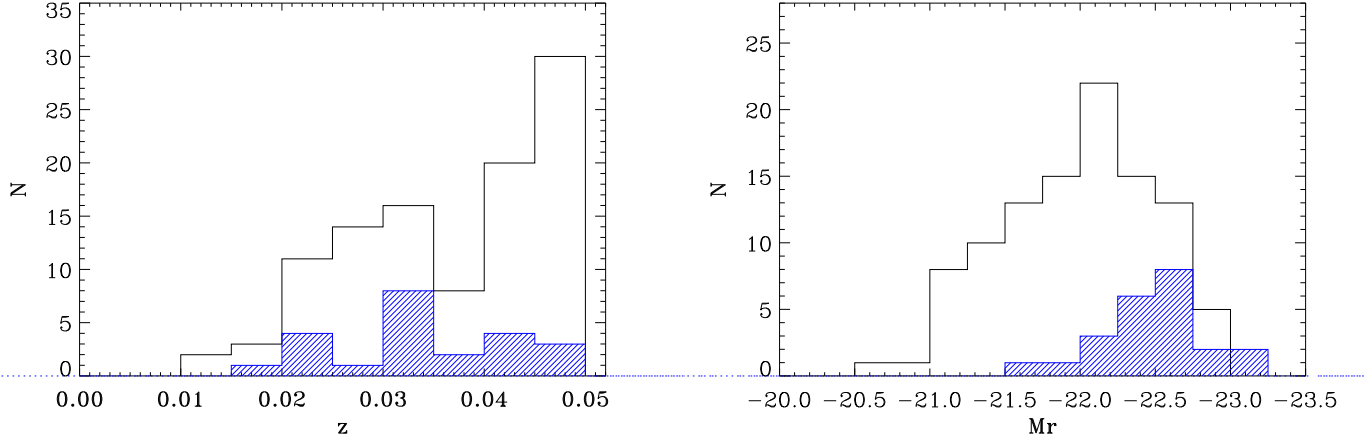


Fig. 1. Left: redshift distribution for the samples of RGs considered, black for the FR 0s, blue shaded for the FR Is, including both FRICAT and sFRICAT objects.

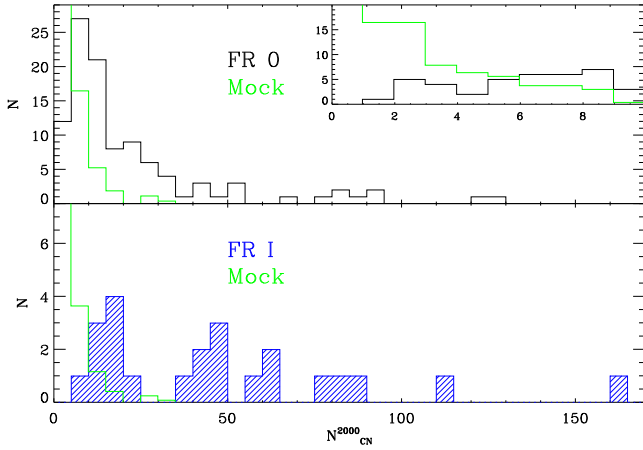


Fig. 2. Top: distribution of the number of cosmological neighbors for the FR 0s; the inset shows the same distribution with a smaller bin size, i.e., 1 instead of 5, to focus on the region of low N_{cn}^{2000} . In green we show the N_{cn}^{2000} distribution for the sample of mock galaxies (see text for details) scaled by a factor 104/287, i.e., normalized to the same area of the FR 0s histogram; the first bin contains 211 MOCKs. The inset is a zoom for low N_{cn}^{2000} for the both FR 0s and MOCKs; the first bin contains 85 MOCKs. Bottom: comparison of the N_{cn}^{2000} distributions for FR Is (blue) and MOCKs (green).

FR Is, and the distributions of this parameter for the two classes differ significantly, see Tab. 1. The same result is obtained when using a radius of 1 Mpc, deriving N_{cn}^{1000} : the medians of this parameter are 7 and 21 for FR 0s and FR Is, respectively.

We compare our results with those derived by cross-correlating our lists of sources with published catalogs of galaxy clusters and groups. More specifically we considered the T12 catalog created by using a modified version of the Friends-of-Friends (FoF) algorithm (Huchra & Geller, 1982; Tago et al., 2010). In Fig. 3 we compare the number of cosmological neighbors, N_{cn}^{2000} , with the number of galaxies, N_{gal} associated with the groups/clusters hosting the radio sources according to T12 (this is possible for all the FR 0s but six, as they are located outside the

area covered by the T12 analysis). There is a general consistency between these two estimates of the galaxies density. However, in several cases N_{gal} is much smaller than N_{cn}^{2000} . For example, there are six objects with $N_{\text{gal}} < 5$ and $N_{\text{cn}}^{2000} > 60$. The field around one of them (namely SDSS J111113.18+284147.0) is shown in the right panel of Fig. 3. T12 finds a group of two galaxies while we found 92 cosmological neighbors, with a strong concentration of sources ~ 200 kpc to the West. We found that by using the FoF algorithm individual clusters of galaxies might be split into multiple sub-structures which are not recognized as being part of a single entity. When looking for the closest group/cluster at a given position, the outcome could be an underestimate of the local galaxies density. This effect is particularly severe at low redshift where structures cover large areas of the sky. In this case, the counting of cosmological neighbors is a more robust method for environmental studies.

We analyzed the fields around the MOCKs with the same strategy used for the RGs. In the bottom panel of Fig. 2 we show as green histogram the resulting distribution of N_{cn}^{2000} which shows a strong concentration for low values of N_{cn}^{2000} . In particular, we find that 95% of the MOCKs correspond to $N_{\text{cn}}^{2000} < 11$. This implies that a value of $N_{\text{cn}}^{2000} > 11$ has a probability of $< 5\%$ to occur by chance. The strong difference in the distributions of N_{cn}^{2000} between FR Is, FR 0s, and the MOCKs (see the insets in the left panel of Fig. 2) indicates that both classes of RGs are located in regions of higher than average galaxies density.

We also estimated the projected galaxies density, following the approach of Dressler (1980), i.e., measuring the Σ_k parameter. Σ_k is defined as the ratio between the number of sources k and the projected area πr_k^2 , where r_k is the projected distance between the central galaxy and the k th nearest neighbor. More specifically, we estimated Σ_5 , derived from the distance of the fifth closest candidate elliptical galaxy. Candidate elliptical galaxies are optical sources lying within the 2 Mpc distance from the RG and having optical colors consistent with those of quiescent ellipticals at the same redshift. The distributions of Σ_5 for FR 0s and FR Is differ significantly, with the latter group showing a median value a factor ~ 3 larger (Fig. 4). The distribution of Σ_5 for the MOCKs has a median a factor ~ 2 lower than the average of the FR 0s. This confirms that, overall, FR 0s are located in an environment richer than average.

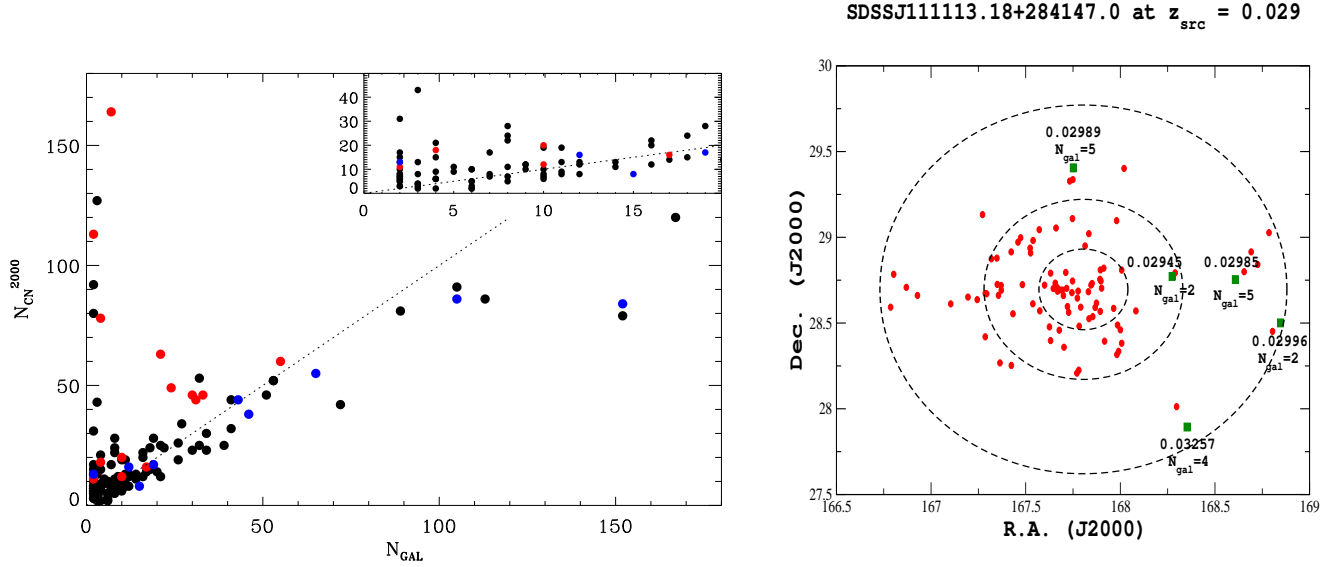


Fig. 3. Left: comparison between the number of cosmological neighbors within a diameter of 2000 kpc (N_{cn}^{2000}) and the number of galaxies (N_{gal}) associated with the groups/clusters hosting the radio sources from T12. Black dots are FR 0s, blue and red are the FRICAT and sFRICAT objects, respectively. The inset in the top right corner is a zoom on the regions of low N_{gal} values. Right: the field around SDSS J111113.18+284147.0 as example of the objects with a large discrepancy between N_{gal} and N_{cn}^{2000} . Cosmological neighbors are shown as red circles, while the green points mark the location of the closest (in projection) groups or clusters of galaxies with a redshift difference $\Delta z < 0.005$, listed in the T12 galaxy cluster/group catalog.

Table 1. Summary of the statistical results

	Average				Median				K.S. (P)
	FR 0	FR I	sFR I	FRICAT	FR 0	FR I	sFR I	FRICAT	
z	0.037	0.035	0.034	0.036	0.039	0.034	0.034	0.032	(0.360)
M_r	-21.97	-22.48	-22.39	-22.63	-22.05	-22.52	-22.39	-22.63	T (0.000)
N_{cn}^{2000}	21.95	47.87	52.86	40.11	13	44	46	38	T (0.002)
N_{cn}^{1000}	13.61	23.91	21.71	27.33	7	21	22	17	T (0.002)
N_{gal}	17.43	30.83	17.86	51.00	8	19	17	43	T (0.001)
$\log \Sigma_5$	-4.74	-4.46	-4.50	-4.39	-4.72	-4.45	-4.45	-4.20	T (0.026)
$N_{\text{cn},0.05}^{2000}$	15.68	23.74	24.07	23.22	8	16	16	15	T (0.016)
$d_{\text{proj}}^{\text{cn}}$	338	347	431	216	303	398	470	190	(0.186)
$-c\Delta z$	235	192	225	141	180	193	259	110	(0.770)

Column description: (1) parameter; (2 - 3) average value for the FR 0s, the FR Is (split into (4 -5) FRICAT and sFRICAT sources); (6 -7) median value for the FR 0s, the FR Is (split into (8 -9) FRICAT and sFRICAT sources) (10) outcome of the Kolmogoroff-Smirnov test (and corresponding probability) T=the FR 0s and FR Is populations differ significantly. The parameters considered are the redshift (z), the source absolute magnitude (M_r), the number of cosmological neighbors within 2 Mpc (N_{cn}^{2000}) and 1 Mpc (N_{cn}^{1000}), the number of galaxies (N_{gal}) associated with the groups/clusters hosting the radio sources according to T12, the fifth nearest neighbor density (Σ_5), the number of cosmological neighbors within 2 Mpc ($N_{\text{cn},0.05}^{2000}$) when all sources are moved to a common redshift of 0.05, the projected distance in kpc ($d_{\text{proj}}^{\text{cn}}$) and the absolute value of the speed of light times the redshift difference in km s^{-1} ($-c\Delta z$) from the average of the cosmological neighbors.

All the estimators concur on the result that the local galaxies density around FR Is is a factor $\sim 2 - 3$ larger than around FR 0s. However, this ratio does not fully capture their different environment. Fig. 2 shows that the main characteristic of the Mpc scale environment is the large fraction of FR 0s located in poor groups of galaxies, an environment which FR Is rarely inhabit. More quantitatively, about 2/3 of the FR 0s (65/104) have $N_{\text{cn}}^{2000} < 15$, while this occurs for only 4 out 23 FR Is (17%).

Despite the similarity in the distance distribution of FR 0s and FR Is we cannot exclude that some residual effect due to redshift is still present and that this affects our results. To address this possibility, we artificially ‘moved’ all sources to a common redshift of 0.05. The magnitudes of each source and of all its cosmological neighbors are re-evaluated by considering the in-

creased distance modulus, with an average correction of ~ 0.7 magnitudes. All neighbors which, after this flux dimming, fall below the threshold of the SDSS spectroscopic selection (i.e., $r > 17.7$) are excluded from the estimates of the local galaxies density. Effectively, this strategy produces a list of cosmological friends with a fixed absolute magnitude limit of $M_r < -19$, with the only drawback of reducing the number of cosmological friends by an average factor 1.5. In Fig. 5 we compare the simulated number of cosmological neighbors within 2 Mpc at a redshift of $z = 0.05$, $N_{\text{cn},0.05}^{2000}$ of FR 0s and FR Is: the two distributions still differ at a high significance level (see Tab. 1).

We considered the possibility of a connection between the properties of the environment, of the active nucleus, and of the host galaxy of the RGs. In particular we tested the presence of a

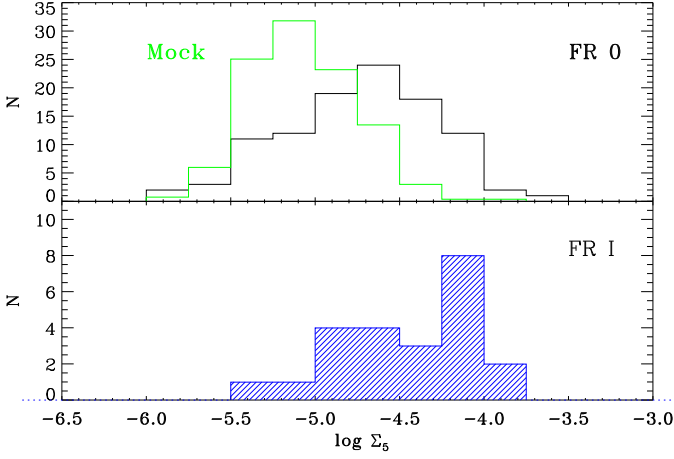


Fig. 4. Comparison of the Σ_5 parameter for (top panel) FR 0s (black) and MOCKs (green, scaled by a factor 104/278), (bottom) distribution of Σ_5 for the FR 1s.

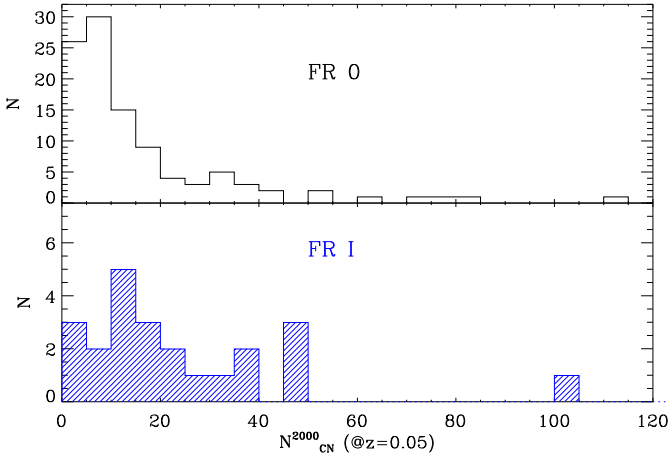


Fig. 5. Distribution of the simulated number of cosmological neighbors for the FR 0s and FR 1s (black and blue histograms, respectively) within 2 Mpc after moving all sources to a common redshift of 0.05.

relation of N_{cn}^{2000} with 1) the [O III] line luminosity, 2) the host black hole mass, and 3) the strength of the Dn(4000) index. The Spearman rank test does not return any significant correlation. The only notable result concerns the five FR 0s forming the tail of low black mass values, $\log M_{BH} < 7.8$, for which we find an even poorer environment than the FR 0s population, with an average value $\bar{N}_{cn}^{2000} = 6.2$.

3.2. Location of the RGs within the group/cluster of galaxies

Using optical observations, the local density of galaxies is not the only parameter which defines the environmental properties as it is also important to establish in which location within a, e.g., cluster of galaxies a given source is located. The location of an AGN within the group/cluster of galaxies might have a profound effect on the level of accretion and, consequently, on its nuclear power (see, e.g., Koulouridis et al. 2018). For example, by exploring the properties of early-type galaxies in the Virgo cluster, Vattakunnel et al. (2010) found a suggestive trend be-

tween jet power and location within the cluster. A similar result was found by Croston et al. (2019).

We then estimated the projected distance, d_{proj}^{cn} , of each RG from the average of the positions in the sky of all its cosmological neighbors within 2 Mpc. Similarly, we estimated the difference between their redshift with respect to the average of the cosmological neighbors, $c\Delta z$. These two quantities are reported in Fig. 6 and a statistical summary is given in Tab. 1. We found $d_{proj}^{cn} < 900$ kpc and $-c\Delta z < 800$ km s⁻¹ for all but three of the RGs considered.

Both the average distance (~ 340 kpc) and the difference in velocity (~ 200 km s⁻¹) are similar for FR 0s and FR 1s and the distributions for the two classes are not statistically distinguishable. The same result is obtained when considering the distribution of cosmological neighbors within 1 Mpc, with $d_{proj}^{cn} = 243$ kpc and 250 kpc for the FR 0s and FR 1s, respectively. There is a difference between the average values between FRICAT and sFRICAT sources, both indicating that the former are closer to the center of the group/cluster, but the small number statistics prevents to draw a firm conclusion. Actually, when restricting to the cosmological neighbors within 1 Mpc this difference disappears.

We also explored the possibility that the location of the radio sources depends on its optical luminosity or on the richness of the galaxies structure. For this reason the symbol sizes in the two panels of Fig. 6 are proportional to N_{cn}^{2000} and M_r , respectively: we do not find any apparent dependency between these quantities. More quantitatively, we experimented whether a cut-off at low values of N_{cn}^{2000} and/or M_r affects the results, but this not the case: in particular the median values of d_{proj}^{cn} and $c\Delta z$ do not change significantly.

We conclude that there is often a large displacement (of the order of 200-300 kpc) of the RGs hosts from the average of the projected location of the cosmological neighbors and that FR 0s and FR 1s do not show significant differences in this respect.

On the other hand the host galaxies of the RGs are invariably the most luminous galaxy among the cosmological neighbors within 2 Mpc. This might an indication of a substantial complexity in the distribution of galaxies, possibly indicative of the presence of sub-structures, not yet completely relaxed. Alternatively, the average of the galaxy locations might not be accurately tracing the location of the center of the galaxies structure.

4. Discussion

The main conclusion on the environmental properties of the three samples of low redshift RGs is that FR 0s live in regions of lower galaxies density with respect to FR 1s, independently on the method used. This is driven by the small fraction of FR 1s located in groups formed by less than 15 galaxies, an environment which, conversely, is typical of FR 0s. The poorer environment of FR 0s with respect to the FR 1s is the first significant difference between these two classes of RGs, leaving aside the defining characteristic of FR 0s, i.e., the lack of substantial extended radio emission.

One possibility to account for the connection between environment and properties of the extended radio emission is related to the adiabatic losses of the radio emitting plasma (e.g., Longair 1994). In a poorer environment density and pressure of the external medium are reduced with respect to regions of higher galaxies density: this causes a faster lateral expansion of the jets, stronger adiabatic losses and, consequently, a re-

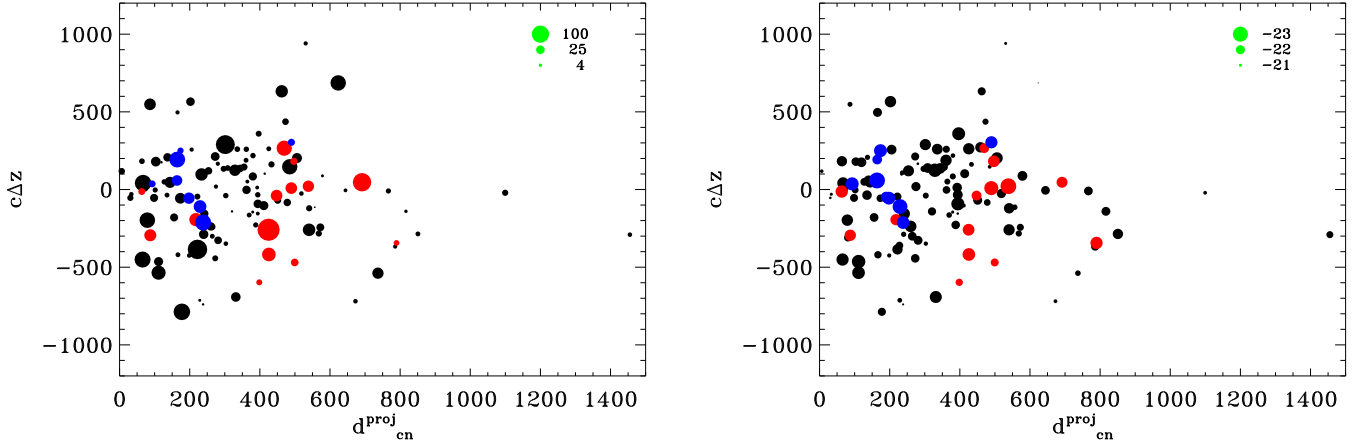


Fig. 6. Projected distance (in kpc) versus the redshift difference times the speed of light (in km s^{-1}) for each RG from the average of its cosmological neighbors. In the left panel the symbol size is proportional to N_{cn}^{2000} (see the coding on the top right) while in the right panel is proportional to the host absolute magnitude.

duced emissivity. However, the high resolution radio observations by Baldi et al. (2019) show that most FR 0s do not reach sizes of even ~ 1 kpc: at these small scales the external gas in which they expand is still well within the core of hot corona of their host. The similarity of the host galaxies of FR 0s and FR Is suggests that also their coronae will have similar properties, based on the connection between optical and X-ray luminosity (Fabbiano et al., 1992). A large spread in the X-ray properties for galaxies of similar absolute magnitude exists, but it does not appear to be closely connected with the local galaxies density (Su et al., 2015). The possibility that the separation between FR 0s and FR Is is driven by differences in their hosts hot gas content appears contrived: the paucity of extended radio emission in FR 0s is more likely to be an intrinsic property of these sources. Nonetheless, it would be important to test this conclusion with X-ray imaging of these low redshift RGs.

Baldi et al. (2015, 2019) suggested that FR 0s are associated with jets of lower bulk Lorentz factor Γ with respect to FR Is, thus reducing their ability to penetrate the ambient medium. Baldi et al. (2015) proposed that a high Γ jet, leading to a FR I morphology, is only produced when the BH spin is close to its maximum value, following the suggestions of a dependence between the BH spin and Γ (McKinney, 2005; Tchekhovskoy et al., 2010; Chai et al., 2012; Maraschi et al., 2012). FR 0s could be associated with BHs of lower spin.

The origin of the connection between BH spin and environment can have two explanations depending on whether the spin evolution is mainly driven by accretion or black hole mergers.

Within the first option, Garofalo & Singh (2019) included the FR 0s into an evolutionary framework for RGs: FR 0s represent the class of sources formed during the transition from highly retrograde spinning (with respect to the accretion disk) BHs associated with the powerful FR IIs, to the prograde BHs of the less powerful FR II LEG or FR I. Garofalo & Singh ascribe the change of BH spin to the angular momentum of the accreting material: a low spin FR 0 evolves into a highly spinning source, i.e., a FR I, when the accreting material reaches $\sim 30\%$ of the initial BH mass. We note that RGs do not need to follow this full evolution, starting as powerful FR IIs: FR 0s might form associated with low spin black holes and then evolve into FR Is. The connection between environment and the classes of RGs

requires, in this scheme, a positive link between local galaxies density and accretion rate. If this is the case, the low BH spin phase would last longer in poorer environment than in regions of higher galaxies density. This would generate a connection between the environment and the jet speed and power. This connection can be seen only on a statistical basis, not on individual objects. In fact, FR 0s would inhabit preferentially a poor environment, but can also be found in clusters of galaxies if they formed recently and do not have yet accreted a sufficient amount of mass onto their central BH to turn into an FR I. Similarly, FR Is might be seen also in poor groups of galaxies. There is evidence that the accretion rate in RGs is controlled by the amount of hot gas available in the circumnuclear regions (Allen et al., 2006; Balmaverde et al., 2008), but the process that would eventually connect the scale at which this is measured (typically $\lesssim 100$ pc) and to the Mpc environment remains to be understood. In this respect, it would be very important to be able to assess the location of RGs with respect the center of the gravitational well.

Alternatively, the BHs spin distribution is set mainly by their mergers history. The simulations performed by Dubois et al. (2014) indicate that indeed the most massive BHs ($M_{\text{BH}} \gtrsim 10^8 M_{\odot}$), in particular those associated with gas poor galaxies (such as the low redshift RGs we are considering), acquire most of their mass through BH coalescence. An analysis of how the BH spin distribution is related to environment, focusing on the massive early-type galaxies, is needed in order to link the observed differences between FR 0s and FR Is to the results of numerical simulations.

5. Summary and conclusions

We compared the environment on Mpc scale of FR 0s and FR Is taking advantage of the information of the local galaxies distribution provided by the SDSS. The samples considered are formed by 104 objects from FR0CAT, 14 from sFRICAT, and 9 from FRICAT (limiting to those with $z < 0.05$, the same redshift limit of the other two samples), the latter two catalogs formed by FR Is of different linear size. The redshift distributions of samples considered do not differ significantly and this enables us

to perform a direct comparison between their environment free from biases due to distance.

Following the methods described in M19, we used as tracer of the local density of galaxies the number of cosmological neighbors, i.e., the galaxies located within a given radius (usually 2 Mpc, but our results are unchanged when using smaller radii, e.g., 1 Mpc) and whose spectroscopic redshift differ by less than 0.005 from the sources of our interest. The median number of cosmological neighbors is a factor ~ 3 larger for FR Is than FR Os. The same conclusion is reached when considering other estimators, the fifth nearest neighbor density Σ_5 or the number of galaxies associated with the RGs according to a catalog of galaxy clusters and groups. This difference is due to the large fraction (63%) of FR Os located in groups of galaxies formed by less than 15 sources, where we only find 17% of the FR Is. The poorer environment of FR Os with respect to the FR Is is the first significant difference found between besides the defining property of FR Os, i.e., the lack of substantial extended radio emission.

The possibility that this link is due stronger adiabatic losses, that might cause a lower jet brightness in FR Os, appears to be contrived: their jets are confined within the hot corona of their hosts and are therefore unaware of the distribution of the external medium on larger scales.

Our results suggest a connection between environment and jet power, driven by a common link with the BH spin. There are two possibilities: low spin RGs (i.e., the FR Os) might evolve into high spin FR Is due to accretion: in an environment of lower density the FR Os phase would last longer. Alternatively, the BH spin distribution results from galaxies mergers and the BH coalescence: the most massive BHs located in gas poor galaxies indeed acquire most of their mass through coalescence. The role of environment on the BH spin evolution remains to be fully investigated.

Our analysis of the environment is only based on optical data. Clearly, X-rays observations of these low redshift RGs are crucial for an independent and complementary analysis of their environment. In fact, the X-rays luminosity and temperature of the inter-galactic medium (IGM) provide an estimate of the total mass of galaxies structures. Furthermore, we found that while both FR Os and FR Is are always associated with the brightest galaxy among the cosmological neighbors, they do not appear to be located at the barycenter of their neighbors. This might an indication that the distribution of galaxies is not yet fully relaxed or that the optical average might not be accurately tracing the location of the center of the galaxies structure. The IGM distribution derived from X-rays images might provide a clearer answer to this problem. Finally, such data would also enable us to compare the properties of the RGs hot coronae in which their jets propagate.

Acknowledgements. We thank M. Volonteri, A. Paggi, I. Pillitteri, and R. Campana, C. C. Cheung and A. Tramacere for useful comments and discussion.

This work is supported by the “Departments of Excellence 2018 - 2022” Grant awarded by the Italian Ministry of Education, University and Research (MIUR) (L. 232/2016). This research has made use of resources provided by the Compagnia di San Paolo for the grant awarded on the BLENV project (S1618_L1_MASF_01) and by the Ministry of Education, Universities and Research for the grant MASF_FFABR_17_01. This investigation is supported by the National Aeronautics and Space Administration (NASA) grants GO4-15096X, AR6-17012X and GO6-17081X. F.M. acknowledges financial contribution from the agreement ASI-INAF n.2017-14-H.0. Funding for SDSS and SDSS-II has been provided by the Alfred P. Sloan Foundation, the Participating Institutions, the National Science Foundation, the U.S. Department of Energy, the National Aeronautics and Space Administration, the Japanese Monbukagakusho, the Max Planck Society, and the Higher Education Funding Council for England. The SDSS Web Site is <http://www.sdss.org/>. The SDSS

is managed by the Astrophysical Research Consortium for the Participating Institutions. The Participating Institutions are the American Museum of Natural History, Astrophysical Institute Potsdam, University of Basel, University of Cambridge, Case Western Reserve University, University of Chicago, Drexel University, Fermilab, the Institute for Advanced Study, the Japan Participation Group, Johns Hopkins University, the Joint Institute for Nuclear Astrophysics, the Kavli Institute for Particle Astrophysics and Cosmology, the Korean Scientist Group, the Chinese Academy of Sciences (LAMOST), Los Alamos National Laboratory, the Max-Planck-Institute for Astronomy (MPIA), the Max-Planck-Institute for Astrophysics (MPA), New Mexico State University, Ohio State University, University of Pittsburgh, University of Portsmouth, Princeton University, the United States Naval Observatory, and the University of Washington.

Appendix A: Appendix

Table A.1. Properties of the FROCAT sample.

name	z	M_r	N_{cn}^{2000}	$N_{\text{cn},0.05}^{2000}$	N_{cn}^{1000}	N_{gal}	$\log \Sigma_5$	$d_{\text{proj}}^{\text{cn}}$	$c\Delta z$
SDSS J010852.48-003919.4	0.045	-21.42	7	7	6	—	-5.34	303	-348
SDSS J011204.61-001442.4	0.044	-21.62	1	0	1	—	-5.91	556	-114
SDSS J011515.78+001248.4	0.045	-21.96	39	30	39	—	-3.71	173	-56
SDSS J015127.10-083019.3	0.018	-21.13	13	7	13	—	-4.04	30	-53
SDSS J020835.81-083754.8	0.034	-22.19	2	2	2	—	-4.59	413	101
SDSS J075354.98+130916.5	0.048	-22.31	11	11	8	14	-5.02	308	138
SDSS J080716.58+145703.3	0.029	-21.82	9	8	8	11	-4.49	101	-3
SDSS J083158.49+562052.3	0.045	-22.00	17	14	2	2	-4.97	354	144
SDSS J083511.98+051829.2	0.046	-22.06	6	6	4	2	-5.37	785	-366
SDSS J084102.73+595610.5	0.038	-22.13	12	8	7	9	-4.35	272	-443
SDSS J084701.88+100106.6	0.048	-22.15	5	5	2	2	-5.65	644	-5
SDSS J090652.79+412429.7	0.027	-21.56	24	9	21	18	-4.20	136	207
SDSS J090734.91+325722.9	0.049	-21.73	13	13	3	3	-5.58	568	-283
SDSS J090937.44+192808.2	0.028	-21.58	30	20	23	34	-4.71	239	-288
SDSS J091039.92+184147.6	0.028	-22.15	8	2	8	10	-4.68	264	-300
SDSS J091601.78+173523.3	0.029	-22.44	42	26	38	72	-4.21	143	46
SDSS J091754.25+133145.5	0.050	-21.14	6	5	3	4	-5.14	280	166
SDSS J093003.56+341325.3	0.042	-22.00	5	4	5	8	-5.03	80	29
SDSS J093346.08+100909.0	0.011	-21.30	14	2	14	17	-5.15	6	118
SDSS J093938.62+385358.6	0.046	-21.70	10	10	2	6	-4.75	302	-39
SDSS J094319.15+361452.1	0.022	-21.79	12	5	12	21	-4.32	72	5
SDSS J100549.83+003800.0	0.021	-21.21	7	3	7	10	-4.31	33	-30
SDSS J101329.65+075415.6	0.046	-22.23	7	6	4	7	-5.11	518	-25
SDSS J101806.67+000559.7	0.048	-21.69	5	4	3	2	-5.13	364	51
SDSS J102403.28+420629.8	0.044	-21.81	19	16	9	10	-4.45	478	-83
SDSS J102511.50+171519.9	0.045	-22.62	34	31	14	27	-4.51	505	202
SDSS J102544.22+102230.4	0.046	-22.15	22	19	5	8	-4.79	155	-179
SDSS J103719.33+433515.3	0.025	-21.98	3	1	2	3	-4.38	80	-309
SDSS J103952.47+205049.3	0.046	-22.18	4	4	2	3	-5.13	816	-140
SDSS J104028.37+091057.1	0.019	-22.07	2	0	2	4	-4.31	320	-140
SDSS J104403.68+435412.0	0.025	-21.77	15	8	12	18	-4.25	264	-240
SDSS J104811.90+045954.8	0.034	-22.29	5	4	5	6	-4.67	392	12
SDSS J104852.92+480314.8	0.041	-22.12	9	7	1	5	-4.95	388	-227
SDSS J105731.16+405646.1	0.025	-22.29	8	5	7	11	-4.41	135	-36
SDSS J111113.18+284147.0	0.029	-22.05	92	54	71	2	-3.93	177	-787
SDSS J111622.70+291508.2	0.045	-22.74	86	75	50	113	-4.43	65	-450
SDSS J111700.10+323550.9	0.035	-22.04	26	18	15	26	-4.31	272	212
SDSS J112029.23+040742.1	0.050	-22.47	19	18	6	11	-5.38	343	135
SDSS J112256.47+340641.3	0.043	-22.93	44	30	21	41	-3.84	328	124
SDSS J112625.19+520503.5	0.048	-21.32	13	11	2	2	-5.40	1099	-20
SDSS J112727.52+400409.4	0.035	-21.20	6	3	3	2	-4.95	530	940
SDSS J113449.29+490439.4	0.033	-22.63	91	53	63	105	-4.25	67	41
SDSS J113637.14+510008.5	0.050	-21.93	8	8	2	2	-5.58	166	-419
SDSS J114230.94-021505.3	0.047	-22.22	6	5	3	4	-5.22	274	19
SDSS J114232.84+262919.9	0.030	-22.58	23	13	16	30	-4.42	241	-155
SDSS J114804.60+372638.0	0.042	-22.54	19	14	10	26	-4.95	253	120
SDSS J115531.39+545200.4	0.050	-21.88	21	21	8	4	-4.85	572	-243
SDSS J120551.46+203119.0	0.024	-21.34	79	39	58	152	-4.18	485	146
SDSS J120607.81+400902.6	0.037	-22.44	13	10	6	11	-5.06	540	-120
SDSS J121329.27+504429.4	0.031	-22.85	12	4	8	9	-4.06	396	359
SDSS J121951.65+282521.3	0.027	-21.12	52	30	37	53	-4.27	233	97
SDSS J122421.31+600641.2	0.044	-22.42	11	8	6	5	-5.38	63	182
SDSS J123011.85+470022.7	0.039	-22.62	24	19	17	22	-4.13	259	-237
SDSS J124318.73+033300.6	0.048	-22.35	10	9	6	9	-5.37	394	-33
SDSS J124633.75+115347.8	0.047	-22.59	8	8	6	12	-4.23	425	262
SDSS J125027.42+001345.6	0.047	-21.23	3	3	3	2	-5.40	379	-145
SDSS J125409.12-011527.1	0.047	-21.87	7	5	1	2	-5.36	1455	-290
SDSS J130404.99+075428.4	0.046	-22.94	28	27	17	19	-4.75	111	-464
SDSS J130837.91+434415.1	0.036	-22.57	53	40	18	32	-4.87	540	-259
SDSS J133042.51+323249.0	0.034	-21.63	43	28	17	3	-4.76	736	-538

Continued on Next Page

Table A.1 – Continued

name	z	M _r	N _{cn} ²⁰⁰⁰	N _{cn,0.05} ²⁰⁰⁰	N _{cn} ¹⁰⁰⁰	N _{gal}	log Σ ₅	d _{proj} ^{cn}	cΔz
SDSS J133455.94+134431.7	0.023	-22.16	14	3	14	20	-4.07	222	-196
SDSS J133621.18+031951.0	0.023	-21.74	12	7	10	12	-4.45	296	133
SDSS J133737.49+155820.0	0.026	-22.32	6	3	6	10	-4.47	205	257
SDSS J134159.72+294653.5	0.045	-22.05	52	44	29	53	-4.82	462	632
SDSS J135036.01+334217.3	0.014	-21.40	7	3	7	8	-4.61	198	-424
SDSS J135226.71+140528.5	0.023	-22.05	12	6	12	16	-4.56	221	-45
SDSS J140528.32+304602.0	0.025	-21.04	2	1	0	6	-4.97	238	-739
SDSS J141451.35+030751.2	0.025	-22.18	20	8	15	16	-4.54	280	-326
SDSS J141517.98-022641.0	0.047	-22.42	8	6	2	2	-5.30	850	-285
SDSS J142724.23+372817.0	0.032	-22.03	22	14	17	16	-4.15	98	-53
SDSS J143156.59+164615.4	0.048	-22.70	31	30	11	2	-4.68	331	-691
SDSS J143312.96+525747.3	0.047	-21.53	46	38	27	51	-4.92	86	548
SDSS J143424.79+024756.2	0.028	-21.35	28	12	19	8	-4.69	411	-103
SDSS J143620.38+051951.5	0.029	-22.19	6	2	3	4	-4.73	165	496
SDSS J144745.52+132032.2	0.044	-21.33	7	7	2	2	-5.14	672	-719
SDSS J145216.49+121711.5	0.031	-21.46	10	3	7	10	-4.86	380	218
SDSS J145243.25+165413.4	0.046	-22.56	120	111	70	167	-4.81	301	289
SDSS J145616.20+203120.6	0.045	-22.59	8	7	3	3	-4.97	360	188
SDSS J150152.30+174228.2	0.047	-22.20	17	14	8	7	-4.54	450	-69
SDSS J150425.68+074929.7	0.049	-21.72	15	13	5	4	-4.85	473	436
SDSS J150601.89+084723.2	0.046	-22.33	3	3	3	6	-5.81	578	87
SDSS J150636.57+092618.3	0.028	-21.12	5	3	4	6	-4.88	394	-154
SDSS J150808.25+265457.6	0.033	-20.63	4	1	3	3	-4.58	304	310
SDSS J152010.94+254319.3	0.034	-22.13	32	21	24	41	-4.44	103	179
SDSS J152151.85+074231.7	0.044	-22.61	81	73	42	89	-4.38	79	-197
SDSS J153016.15+270551.0	0.033	-21.51	13	8	9	12	-4.68	433	161
SDSS J154147.28+453321.7	0.037	-21.98	24	15	8	8	-5.41	361	-2
SDSS J154426.93+470024.2	0.038	-22.49	11	8	6	8	-4.81	335	259
SDSS J154451.23+433050.6	0.037	-22.43	15	13	7	2	-5.34	458	271
SDSS J155951.61+255626.3	0.045	-21.99	10	7	5	2	-5.25	127	49
SDSS J155953.99+444232.4	0.042	-21.88	10	10	3	6	-4.78	361	259
SDSS J160426.51+174431.1	0.041	-20.89	80	63	34	2	-4.68	623	686
SDSS J160523.84+143851.6	0.041	-22.60	25	18	8	21	-5.19	202	565
SDSS J160641.83+084436.8	0.047	-22.16	9	5	6	4	-4.72	766	-9
SDSS J161238.84+293836.9	0.032	-21.71	23	16	17	34	-4.57	380	84
SDSS J161256.85+095201.5	0.017	-21.49	2	0	2	3	-4.24	235	108
SDSS J162146.06+254914.4	0.048	-22.49	13	10	11	14	-4.67	140	55
SDSS J162846.13+252940.9	0.040	-21.97	25	19	19	32	-4.74	227	-360
SDSS J162944.98+404841.6	0.029	-18.99	127	82	92	3	-4.08	222	-385
SDSS J164925.86+360321.3	0.032	-21.63	8	5	5	7	-4.62	369	-164
SDSS J165830.05+252324.9	0.033	-21.49	3	1	3	2	-4.74	228	-713
SDSS J170358.49+241039.5	0.031	-22.31	2	2	2	6	-4.78	119	175
SDSS J171522.97+572440.2	0.027	-22.81	67	39	52	—	-4.10	111	-535
SDSS J172215.41+304239.8	0.046	-22.87	25	22	19	39	-4.54	394	-92

Column description: (1) source name; (2) redshift; (3) SDSS DR7 r band AB absolute magnitude; (4 and 5) number of cosmological friends within 2 Mpc, observed and simulated at z=0.05, respectively; (6) number of cosmological friends within 1 Mpc; (7) N_{gal} from T12; (8) fifth nearest neighbor density Σ₅; (9 and 10) projected distance in kpc (d_{proj}^{cn}) and redshift difference (times the speed of light) in km s⁻¹ (cΔz) from the average of the cosmological neighbors.

Table A.2. Properties of the sFRICAT sources.

name	z	M_r	N_{cn}^{2000}	$N_{\text{cn},0.05}^{2000}$	N_{cn}^{1000}	N_{gal}	$\log \Sigma_5$	$d_{\text{proj}}^{\text{cn}}$	$c\Delta z$
SDSS J090100.09+103701.7	0.029	-22.54	11	2	3	2	-5.38	789	-343
SDSS J092122.11+545153.9	0.045	-22.35	60	47	27	55	-4.77	217	-193
SDSS J092151.48+332406.5	0.024	-22.12	78	21	43	4	-4.45	469	266
SDSS J093957.34+164712.8	0.047	-21.71	12	11	7	10	-4.19	398	-597
SDSS J101623.01+601405.6	0.031	-22.55	16	10	15	17	-4.82	63	-13
SDSS J104740.48+385553.6	0.035	-22.84	46	24	22	33	-4.38	489	9
SDSS J111125.21+265748.9	0.034	-22.61	63	16	16	21	-3.85	425	-418
SDSS J132451.44+362242.7	0.017	-21.83	20	4	10	10	-4.17	499	-469
SDSS J133242.54+071938.1	0.023	-22.15	46	12	21	30	-4.05	447	-39
SDSS J145222.83+170717.8	0.045	-22.32	113	100	37	2	-4.81	691	46
SDSS J155603.90+242652.9	0.043	-22.44	18	10	9	4	-4.69	496	181
SDSS J155749.61+161836.6	0.037	-23.12	44	26	26	31	-4.80	538	21
SDSS J160332.08+171155.2	0.034	-22.46	164	38	44	7	-4.16	424	-259
SDSS J160722.95+135316.4	0.034	-22.39	49	16	24	24	-4.49	87	-294

Table A.3. Properties of the FRICAT sources with $z < 0.05$.

name	z	M_r	N_{cn}^{2000}	$N_{\text{cn},0.05}^{2000}$	N_{cn}^{1000}	N_{gal}	$\log \Sigma_5$	$d_{\text{proj}}^{\text{cn}}$	$c\Delta z$
SDSS J100451.83+543404.3	0.047	-22.63	44	39	17	43	-4.64	197	-55
SDSS J103258.88+564453.2	0.045	-22.96	55	45	36	65	-4.09	229	-109
SDSS J104921.13-004005.0	0.039	-22.65	13	9	8	2	-5.23	173	250
SDSS J113359.23+490343.4	0.032	-22.62	86	46	60	105	-4.00	238	-212
SDSS J120401.47+201356.3	0.024	-22.11	84	31	70	152	-4.00	164	192
SDSS J141652.94+104826.7	0.025	-23.14	38	15	31	46	-4.05	163	58
SDSS J145555.27+115141.4	0.032	-22.52	17	8	9	19	-4.60	490	304
SDSS J155721.38+544015.9	0.047	-22.68	16	12	9	12	-4.20	92	36
SDSS J161114.11+265524.2	0.032	-22.31	8	4	6	15	-4.68	189	-49

Column description: (1) source name; (2) redshift; (3) SDSS DR7 r band AB absolute magnitude; (4 and 5) number of cosmological friends within 2 Mpc, observed and simulated at $z=0.05$, respectively; (6) number of cosmological friends within 1 Mpc; (7) N_{gal} from T12; (8) fifth nearest neighbor density Σ_5 ; (9 and 10) projected distance in kpc ($d_{\text{proj}}^{\text{cn}}$) and redshift difference (times the speed of light) in km s^{-1} ($c\Delta z$) from the average of the cosmological neighbors.

References

- Ahn, C. P., Alexandroff, R., Allende Prieto, C., et al. 2012, *ApJS*, 203, 21
- Allen, S. W., Dunn, R. J. H., Fabian, A. C., Taylor, G. B., & Reynolds, C. S. 2006, *MNRAS*, 372, 21
- Baldi, R. D. & Capetti, A. 2009, *A&A*, 508, 603
- Baldi, R. D., Capetti, A., & Giovannini, G. 2015, *A&A*, 576, A38
- Baldi, R. D., Capetti, A., & Giovannini, G. 2019, *MNRAS*, 482, 2294
- Baldi, R. D., Capetti, A., & Massaro, F. 2018, *A&A*, 609, A1 (BCM18)
- Balmaverde, B., Baldi, R. D., & Capetti, A. 2008, *A&A*, 486, 119
- Becker, R. H., White, R. L., & Helfand, D. J. 1995, *ApJ*, 450, 559
- Bennett, C. L., Larson, D., Weiland, J. L., & Hinshaw, G. 2014, *ApJ*, 794, 135
- Best, P. N. 2004, *MNRAS*, 351, 70
- Best, P. N. & Heckman, T. M. 2012, *MNRAS*, 421, 1569
- Best, P. N., Kauffmann, G., Heckman, T. M., & Ivezić, Ž. 2005, *MNRAS*, 362, 9
- Capetti, A., Massaro, F., & Baldi, R. D. 2017, *A&A*, 598, A49
- Chai, B., Cao, X., & Gu, M. 2012, *ApJ*, 759, 114
- Cheng, X.-P. & An, T. 2018, *ApJ*, 863, 155
- Condon, J. J., Cotton, W. D., Greisen, E. W., et al. 1998, *AJ*, 115, 1693
- Croston, J. H., Hardcastle, M. J., Mingo, B., et al. 2019, *A&A*, 622, A10
- Dressler, A. 1980, *ApJ*, 236, 351
- Dubois, Y., Volonteri, M., & Silk, J. 2014, *MNRAS*, 440, 1590
- Eke, V. R., Baugh, C. M., Cole, S., et al. 2004, *MNRAS*, 348, 866
- Fabbiano, G., Kim, D.-W., & Trinchieri, G. 1992, *ApJS*, 80, 531
- Fanaroff, B. L. & Riley, J. M. 1974, *MNRAS*, 167, 31P
- Garofalo, D. & Singh, C. B. 2019, *ApJ*, 871, 259
- Gendre, M. A., Best, P. N., Wall, J. V., & Ker, L. M. 2013, *MNRAS*, 430, 3086
- Ghisellini, G. 2011, in *American Institute of Physics Conference Series*, Vol. 1381, *American Institute of Physics Conference Series*, ed. F. A. Aharonian, W. Hofmann, & F. M. Rieger, 180–198
- Hardcastle, M. J., Alexander, P., Pooley, G. G., & Riley, J. M. 1998, *MNRAS*, 296, 445
- Helfand, D. J., White, R. L., & Becker, R. H. 2015, *ApJ*, 801, 26
- Hill, G. J. & Lilly, S. J. 1991, *ApJ*, 367, 1
- Huchra, J. P. & Geller, M. J. 1982, *ApJ*, 257, 423
- Koulouridis, E., Ricci, M., Giles, P., et al. 2018, *A&A*, 620, A20
- Laing, R. A., Jenkins, C. R., Wall, J. V., & Unger, S. W. 1994, in *Astronomical Society of the Pacific Conference Series*, Vol. 54, *The Physics of Active Galaxies*, ed. G. V. Bicknell, M. A. Dopita, & P. J. Quinn, 201
- Longair, M. S. 1994, *High energy astrophysics*, Cambridge University Press
- Longair, M. S. & Seldner, M. 1979, *MNRAS*, 189, 433
- Maraschi, L., Colpi, M., Ghisellini, G., Perego, A., & Tavecchio, F. 2012, *Journal of Physics Conference Series*, 355, 012016
- Massaro, F., Álvarez-Crespo, N., Capetti, A., et al. 2019a, *ApJS*, 240, 20
- Massaro, F., Álvarez-Crespo, N., Capetti, A., et al. 2019b, *ApJS*, 240, 20 (M19)
- McKinney, J. C. 2005, *ApJ*, 630, L5
- Prestage, R. M. & Peacock, J. A. 1988, *MNRAS*, 230, 131
- Sadler, E. M., Ekers, R. D., Mahony, E. K., Mauch, T., & Murphy, T. 2014, *MNRAS*, 438, 796
- Spinrad, H., Marr, J., Aguilar, L., & Djorgovski, S. 1985, *PASP*, 97, 932
- Su, Y., Irwin, J. A., White, III, R. E., & Cooper, M. C. 2015, *ApJ*, 806, 156
- Tago, E., Saar, E., Tempel, E., et al. 2010, *A&A*, 514, A102
- Tchekhovskoy, A., Narayan, R., & McKinney, J. C. 2010, *ApJ*, 711, 50
- Tempel, E., Saar, E., Liivamägi, L. J., et al. 2011, *A&A*, 529, A53
- Tempel, E., Tago, E., & Liivamägi, L. J. 2012, *A&A*, 540, A106
- Torresi, E., Grandi, P., Capetti, A., Baldi, R. D., & Giovannini, G. 2018, *MNRAS*, 476, 5535
- van Haarlem, M. P., Wise, M. W., Gunst, A. W., et al. 2013, *A&A*, 556, A2
- Vattakunnel, S., Trussoni, E., Capetti, A., & Baldi, R. D. 2010, *A&A*, 522, A89